Synthesis and Characterization of Mesoporous Niobium-Doped Silica Molecular Sieves

Lei Zhang and Jackie Y. Ying
Dept. of Chemical Engineering, Massachusetts Institute of Technology, Cambridge, MA 02139

Hexagonally-packed mesoporous Nb-doped silica molecular sieves were hydrothermally synthesized with various siliceous sources and dopant concentration levels. The microstructure of mesoporous materials was characterized by a variety of physico-chemical methods. The pore packing order of the Nb-doped material depended strongly on the synthesis conditions such as aging temperature, pH of reaction mixture, surfactant-to-Si ratio, and dopant concentration. Different silica precursors gave rise to different reactivity with the Nb dopants and interactions with the surfactants. The pore size and surface area of the materials can be systematically varied. The chemical environment of the Nb dopants in the silica framework was studied by XPS, EPR, PA-FTIR, UV-Vis, and ^{29}Si MAS NMR. The results indicated that the Nb^{5+} ions were well dispersed in the framework of the mesoporous silica. The diffuse-reflectance UV-Vis spectrum of the mesoporous Nb-doped silica is red-shifted with respect to pure mesoporous silica. The ^{29}Si MAS NMR spectrum contained a broad component at about -105 ppm, which may have been attributed to the presence of Nb-O-Si bonding in the mesostructure.

Introduction

Mesoporous materials with a well-defined pore structure have recently attracted a great deal of research attention due to their potential in separations and catalytic applications. Compared with microporous molecular sieves which have pore sizes less than 2 nm, mesoporous materials have large pore dimensions (2-10 nm) that allow for free diffusion of bulky organic molecules. A great deal of recent research interests have been focused on the well-defined mesoporous molecular sieves belonging to the M41S family (Kresge et al., 1992; Beck et al., 1992; Chen et al., 1993; Tanev and Pinnavaia, 1995, 1996; Antonelli and Ying, 1996a; Brinker, 1996; Huo et al., 1996; Sayari, 1996; Stucky et al., 1996; Zhao et al., 1996). Significant benefits can be obtained by increasing the compositional flexibility of the silicate-based system through the derivation of multicomponent mesoporous oxides.

The ability to tailor pore structures and control chemical composition in novel materials represents an important frontier in catalysis research. Isomorphous substitution of silica with a transition metal is an excellent strategy in creating catalytically active sites and anchoring sites for catalytically active molecules in the design of new heterogeneous catalyst. Several successful examples of doped mesoporous silicates have been demonstrated with metals such as aluminum, titanium, manganese, iron, boron, and vanadium (Reddy et al., 1994; Luan et al., 1995; Tanev et al., 1994; Zhao et al., 1995; Yuan et al., 1995; Sayari et al., 1995). Doping molecular sieves with metals can significantly affect the catalytic behavior and lead to new catalysts with improved properties. For example, Ti-doped MCM-41 has been shown to be highly selective for the hydroxylation of aromatics (Corma et al., 1994; Tanev et al., 1994; Zhang et al., 1996). In addition, the high surface area mesoporous materials can be used as a support for catalytically active molecules. An interaction between the support and the catalytic species can normally be established based on either ion-exchange or ligand coordination on the internal surface of the mesoporous material. For example, aluminosilicate MCM-41 has been used to host iron (II) phenanthroline for the hydroxylation of phenol (Liu et al., 1996). This supported catalyst prepared by an impregnation method showed a higher catalytic activity than its homogeneous counterpart.

To strengthen the catalyst-support interaction, the creation of covalent bonds between the catalyst and the support would be highly desirable. This could be achieved through the manipulation of the surface coordination chemistry. For exam-

Correspondence concerning this article should be addressed to J. Y. Ying.

ple, the introduction of suitable transition metal dopants into the framework of MCM-41 would allow for ligation with specific functionalities of catalytic complexes. Recently, the successful synthesis of Nb-TMS1 (the niobium oxide analogue of MCM-41) via a ligand-assisted templating mechanism (LAT) demonstrated a strong interaction between the amine surfactant molecules and the transition metal precursor for structure-directing purposes during surfactant self-assembly (Antonelli et al., 1996; Antonelli and Ying, 1996a,b). Using a similar concept that involves Nb-N covalent bonding, we have established a unique design rationale for fixating a metalloporphyrin containing amine groups [iron(III) meso-(tetraaminophenyl)porphyrin bromide] in an Nb-doped MCM-41 (Zhang et al., 1997). The resulting heterogeneous catalyst is shown to overcome the common leaching problem found with supported metalloporphyrin catalysts. To optimize the catalytic performance of this heterogeneous catalyst and study the structure-property relationship, it is important to control the microstructure of the Nb-doped mesoporous materials and to examine the nature of the Nb dopant in the mesoporous silicate framework.

In this article, a series of Nb-doped mesoporous materials was synthesized under systematically varied conditions. Characterization of the nature of the Nb dopant in the mesoporous silica was accomplished through various spectroscopic techniques. The results indicated that the Nb^{5+} species were highly dispersed in the framework of the mesoporous silica. The surface-exposed Nb atoms were easily accessible for coordination with guest molecules, making this material an excellent catalyst support.

Experimental Studies

Synthesis

The Nb-doped mesoporous silica was synthesized under both basic and acidic conditions, based on the interaction between an inorganic siliceous precursor and a cationic alkyltrimethylammonium surfactant $[C_nH_{2n+1}(CH_3)_3NBr]$. The siliceous sources used in the synthesis were a 10-wt. % aqueous tetramethylammonium silicate (TMAS) solution (Sachem), a 27-wt. % sodium silicate solution (Aldrich), and tetraethoxysilane (TEOS) (Alfa Aesar). In the first case, 1.82 g of cetyltrimethylammonium bromide (CTMABr) (Alfa) dissolved in 21.6 g of water was mixed with 22.4 g of TMAS solution at room temperature and stirred for 30 min. In the second case, 3.65 g of CTMABr was completely dissolved in 166 g of water. To this solution, 22.2 g of sodium silicate solution diluted in 50 g of water was slowly added at room temperature with vigorous stirring for 30 min. In both cases, a gel-like precipitate was obtained. A desired amount of the Nb-dopant precursor, niobium ethoxide $[Nb(OEt)_5]$ (Aldrich), was gradually introduced into the loosely-bonded silica gel. The pH of the mixture was adjusted to 11.5 by the addition of dilute H_2SO_4. The resulting gel mixture was stirred continuously for 3 hours at ambient conditions before subjected to a hydrothermal treatment within a temperature range of $75-150$°C for a desired period of time.

The third route of doped MCM-41 preparation involves a low-pH synthesis. Acidic conditions were applied when TEOS was used as a siliceous source to promote the formation of monosilicic acid by rapid hydrolysis of TEOS (Brinker and Scherer, 1990; Ying et al., 1993). The cationic silicate species could interact with cationic surfactants via a charge tri-layer ($S^+X^-I^+$) with a halide X^- as a mediating ion, forming SBA-3 (Huo et al., 1994a,b; Firouzi et al., 1995). For this synthesis route, 37.3 g of 48-wt. % HBr was diluted in 32.5 g of water, and 1.391 g of CTMABr was dissolved in this acidic media with vigorous stirring. Then, 5 g of TEOS was slowly introduced with stirring to form a yellowish sol. The amount of niobium ethoxide required to obtain the desired Si/Nb ratio was then added to the silica sol and stirred at room temperature for 24 hours. In all three cases, the molar composition of the gel was represented as 1 SiO_2: xCTMABr: 120 H_2O: yNb_2O_5 (where $x = 0.1-2$ and $y = 0-0.15$). The crystallized solid was washed with ethanol and water, filtered, and then calcined at 540°C in air for 6 hours to remove the organic surfactants. In some cases, mesitylene was used as a swelling agent to enlarge the pores of Nb-doped silica. The Nb-doped mesoporous silicate samples obtained from the TMAS, sodium silicate and TEOS precursors described above are designated as NbSi1-*R*, and NbSi2-*R* and NbSi3-*R*, respectively, where *R* is given by the precursor atomic ratio of Si and Nb. Except where otherwise specified, the NbSi1-*R*, NbSi2-*R* and NbSi3-*R* samples were synthesized with a surfactant-to-Si ratio of 0.5, 0.1 and 0.24, respectively. A series of samples were prepared by systematically varying the synthesis temperature, solution pH, dopant concentration, and surfactant-to-silica molar ratio.

Characterization

The regularity of pore structure of the Nb-doped mesoporous silica was characterized by powder X-ray diffraction (XRD) (Siemens D5000 θ-θ diffractometer), operated at 45 kV and 40 mA using Ni-filtered CuK_α radiation. The chemical composition of the Nb-doped mesoporous silica was determined by direct current plasma emission spectroscopy (Luvak Inc.). The mesoporous structure was examined with transmission electron microscopy (TEM) using a lanthanum hexaboride (LaB_6) filament (JOEL 200CX, 200 kV). The N_2 adsorption analysis was performed on an ASAP 2010 gas sorption instrument (Micromeritics). The BET (Brunauer-Emmett-Teller) (Gregg and Sing, 1982), and BJH (Barrett-Joyner-Halenda) (Barrett et al., 1951) methods were used to calculate the samples' surface area and pore size distribution, respectively. Thermal evolution of the materials was investigated by thermal gravimetric analysis (TGA) (Perkin Elmer TGA7). Chemical bonding in the mesoporous materials was studied by photoacoustic Fourier-transform infrared (PA-FTIR) spectroscopy. Spectra were collected in a 2.5-kHz rapid scan mode at 2-cm^{-1} resolution using an MTEC Model 200 photoacoustic cell in a Bio-Rad FTS-60A/896 spectrometer.

To evaluate the acidity of the mesoporous materials, the adsorption of pyridine was studied *in situ* using a Harrick HVC-DRA2 diffuse-reflectance infrared Fourier-transform (DRIFT) cell on the Bio-Rad FTS-60A/896 spectrometer. The mesoporous material was purged under He at 500°C for 3 hours followed by exposure to pyridine vapor for 1 hour at 150°C. The spectra of sample were then collected after 30 min of purging with He in a temperature range of $150-300$°C. Diffuse-reflectance UV-Vis spectra were obtained on a Cary 5E spectrometer operating using polytetrafluoroethylene

plate as a reference. The sample was ground into a fine powder and compressed into a 1/2-in.-dia. (12.7-mm-dia.) pellet using a hydraulic press at 15,000 lb (6.8 Mg). Solid state ^{29}Si magic angle spinning nuclear magnetic resonance (MAS NMR) spectra were acquired on a 270-MHz spectrometer (^{29}Si resonance 53.762 MHz) with tetramethylsilane as the reference (Spectral Data Service). Ambient electron spin resonance (ESR) spectra were recorded at X-band (frequency 9.34 GHz) on a Bruker ESP 300 spectrometer. X-ray photoelectron (XPS) spectra were collected on a SSX-100 XPS spectrometer (Surface Science Laboratory) with an AlK_α X-ray source. The powder sample was lightly dusted onto a sample holder with a polymer film-based double-sided adhesive tape. A small metallic mesh was applied onto the sample to minimize disturbance of the powder surface during the evacuation of the analysis chamber.

Results and Discussion

Microstructure of the Nb-doped mesoporous silica

Comparison of Different Synthesis Routes. The Nb-doped mesoporous material prepared by different methods showed different textural and structural characteristics. The calcined NbSi1-20 and NbSi2-20 samples which have been aged at 100°C for 4 days gave well-defined hexagonal XRD patterns (Figures 1a and 1b) associated with highly-ordered pore packing. The NbSi3-20 sample showed only a broad (100) diffraction (Figure 1c). The absence of diffraction peaks at higher 2θ values may be due to a poorly-defined pore packing in this material. The TEM micrographs, shown in Figure 2, clearly display a hexagonally-packed porous array with approximate average diameters of 27 Å and 26 Å for the NbSi1-20 and NbSi2-20 samples, respectively. The surface areas and average pore sizes obtained from N_2 adsorption are summarized in Table 1. The N_2 adsorption-desorption analysis for NbSi1-20 and NbSi2-20 showed Type IV isotherms with little hysteresis (Figure 3) typical of mesoporous MCM-41 and narrow pore size distributions (Figure 4) centered at 28 Å and 23 Å, respectively. We note that the surface areas of the mesoporous materials differ greatly depending on their synthesis routes.

In the self-assembly mechanism of MCM-41 (Beck et al., 1992; Huo et al., 1994), the inorganic molecules are involved in a charge matching interaction with the surfactant templating molecules and their counterions. At the surfactant-to-Si ratios (< 1) used for high pH routes, the hexagonal MCM-41 phase was formed, consistent with Beck et al.'s observation (1994). The differences in the microstructure of these materials can be attributed to the nature of the silica source that plays an important role in the mesostructure formation. At a given sol pH, different siliceous species in the reaction medium have a different relative reactivity with the dopant precursors and a different effect on the ordering of the surfactant molecules to the desired mesostructure. In zeolite synthesis, different crystalline structures could be obtained by varying silica sources due to the size and structure of the silicate species in the reaction media. The chemistry of the organic-based silicate, TMAS, differs from that of the sodium silicate solution in that the former contains more colloidal silica in solution stabilized by an adsorbed monolayer of $(CH_3)_4N^+$ (Beard, 1973). This monolayer interferes with the condensation of the silica and slows down the precipitation/gelation and particle growth (Iler, 1979). The $(CH_3)_4N^+$-surrounded silica species further interacts with long-chain cationic surfactants as the $CTMA^+$ can ion-exchange with the surface $(CH_3)_4N^+$ cations, facilitating the organic-inorganic interaction. We could consider the geometry of the surfactant adjacent to $(CH_3)_4N^+$ to be similar to a divalent ammonium surfactant with a $C_{16\text{-}2\text{-}1}$ molecular shape (Huo et al., 1996). The effective head group area of the surfactant would be doubled with the $(CH_3)_4N^+$ cations incorporated, increasing the total micellar volume. As a result, the pore diameter of the mesoporous NbSi1-*R* materials is larger than the other samples (see Table 1). In the sodium silicate case, Na^+ cations are too small to affect the micellar volume during the mesostructure formation.

Acidic synthesis route involving low surfactant concentration and low aging temperature has been developed for producing mesoporous silica and supported silica thin film (Schacht et al., 1996; Yang et al., 1996). It provides a conve-

Table 1. Microstructure of the Mesoporous Nb-Doped Silicates

Sample	Surface Area (m^2/g)*	Pore Vol. (cm^3/g)*	Avg. Pore Dia. (Å)*	Unit Cell (a_o) (Å)**	Wall Thickness (Å)
NbSi1-20	1,122	1.1	28	46.2	18.2
NbSi2-20	822	0.7	23	41.6	18.6
NbSi3-20	694	0.5	< 17	49.9	—

*From N_2 adsorption analysis.
**From XRD analysis.

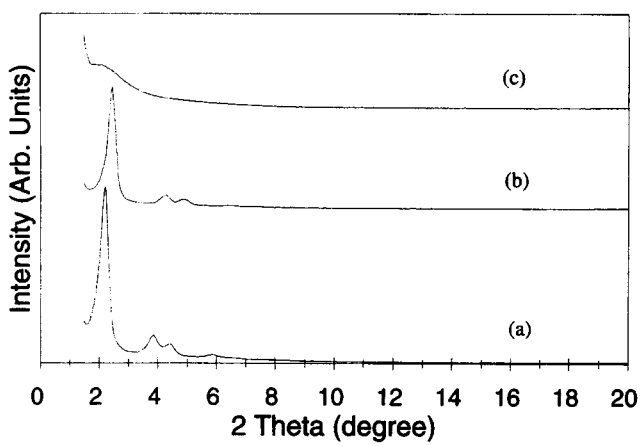

Figure 1. XRD patterns of (a) NbSi1-20, (b) NbSi2-20, and (c) NbSi3-20.

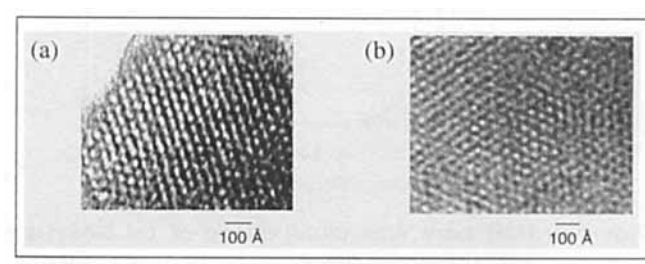

Figure 2. TEM images of (a) NbSi1-20 and (b) NbSi2-20.

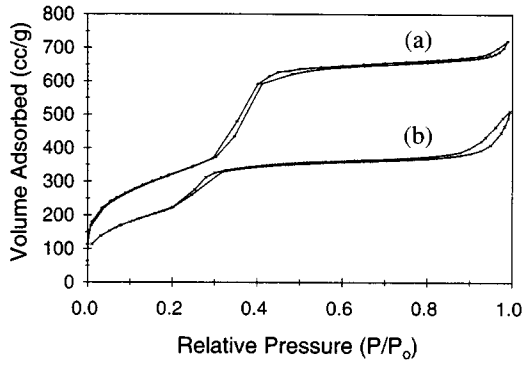

Figure 3. N_2 adsorption-desorption isotherms of (a) NbSi1-20 and (b) NbSi2-20.

nient process to derive high-quality mesoporous materials. When TEOS is used as the siliceous source, its neutral pH and immiscibility in aqueous solution would only give rise to a weak interaction with the cationic surfactants. This silicate precursor tends to form a bulk amorphous gel without mesostructure formation at a pH of 10-12. In contrast, a strongly acidic condition leads to rapid hydrolysis of the TEOS to silicic acid and relatively slow condensation, which is favorable toward mesostructure development. When $Nb(OEt)_5$ is introduced, its alkoxy groups undergo rapid hydrolysis in the presence of water. A freshly-precipitated niobium oxyhydroxide gel then results from partial condensation via an olation/oxolation between Nb species (Faiberother, 1967; Alquier et al., 1986). In the binary system, it is not favorable to have one alkoxide reacting much faster than another alkoxide precursor when molecular homogeneity is desired. The rapid precipitation of niobium oxyhydroxide, which interferes with self-assembly of inorganic species under the acidic conditions examined, did not allow well-defined mesostructure to be developed. It is also expected that the bridging Si-O-Nb bonds are not likely to be derived in this case for a uniformly doped sample.

Effect of Dopant Concentration. In the synthesis of Nb-doped mesoporous silica, the microstructure of the materials was greatly affected by the dopant concentration. At a given aging temperature, the unit cell parameter calculated by $a_0 = 2d_{100}/\sqrt{3}$ (Oster and Riley, 1952) is larger for Nb-doped

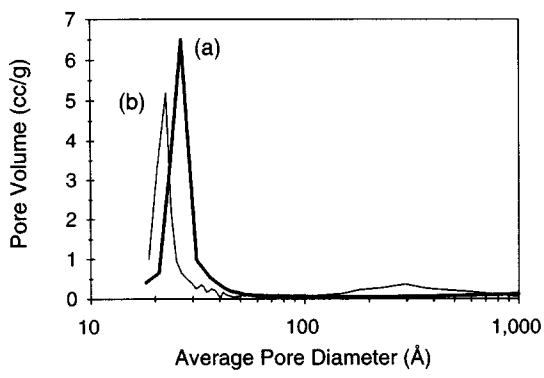

Figure 4. BJH pore size distributions of (a) NbSi1-20 and (b) NbSi2-20 obtained from the adsorption branch of their nitrogen isotherms.

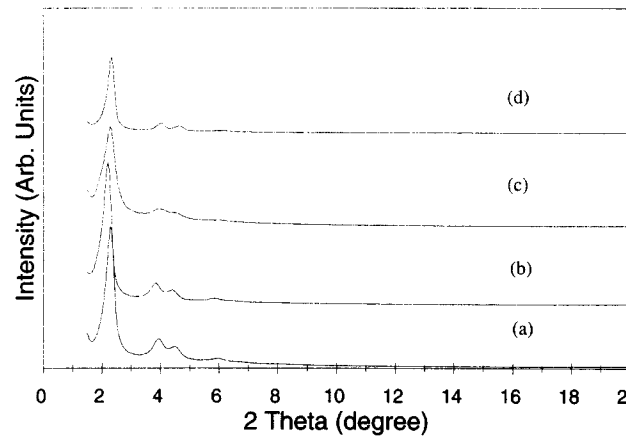

Figure 5. XRD patterns of NbSi1-*R* samples at different dopant concentrations: (a) $R = 10$, (b) $R = 20$, (c) $R = 100$, and (d) $R = \infty$ (pure mesoporous silica).

silica ($R \geq 20$) (Figures 5b and 5c) than for the mesoporous pure SiO_2 (Figure 5d) and increases with an increase in the Nb dopant concentration due to the larger ionic radius of Nb^{5+} (0.64 Å) and longer Nb-O bond length (1.69 Å). However, a decrease in the $d(100)$ spacing was observed at high Nb-dopant concentrations ($R < 20$) (Figure 5a). This may indicate a strong interaction of the Nb precursor with the inner silica walls, providing a high surface Nb concentration. Similar results have been reported for V-MCM-48 and Ti-modified MCM-41 systems (Morey et al., 1996; Schwarz et al., 1996).

This suggests that the mechanism of Nb incorporation involves two stages. In the initial stage, the condensation of silicate species is slow at low temperatures (Brack and Flanigen, 1968). Previous studies showed that mesoporous silica obtained at this early stage has the characteristics of a salt which could redissolve in the aqueous solution (Huo et al., 1994a). Therefore, the framework of such loosely-bonded silica gel has the flexibility of incorporating heteroatoms. The partially-reacted Nb precursor at room temperature can be incorporated into the silica framework at this stage. That the sample obtained after aging for 3 hours showed a hexagonally-packed XRD pattern with broader peaks and a smaller $d(100)$ spacing than that aged for 4 days confirms the gradual evolution of the mesostructure. During the second stage of synthesis, the Nb polyanions become fully condensed into the lattice of the strengthened silica framework under the high-temperature hydrothermal conditions.

Elemental analysis of the samples (Table 2) showed that more of the Nb precursor was incorporated in the framework when sodium silicate was used as the siliceous source instead of TMAS. This can be explained by the faster hydrolysis and condensation rates of sodium silicate when compared to that of TMAS. Since the reactivity of $Nb(OEt)_5$ is higher than that of the silica precursors, a better match of the reaction rates is helpful toward Nb incorporation into the silica framework. The long-range order and regularity of the pore packing were found to decrease with increasing dopant concentration. To maintain the well-defined long-range ordering of the mesostructure during the polymerization of the inorganic

Table 2. Elemental Analysis of the Mesoporous Nb-Doped Silicates

R = Si/Nb (Precursor Atomic Ratio)	NbSi1-R			NbSi2-R		
	Nb (wt. %)	Si (wt. %)	Si/Nb*	Nb (wt. %)	Si (wt. %)	Si/Nb*
100	1.44	43.2	100	2.07	43.3	69
20	2.28	42.4	62	3.21	43.6	45
10	3.85	41.5	36	9.36	38.9	14

*Atomic ratio from elemental analysis.

species, the heteroatoms must be able to organize on the same kinetic time scale as the siliceous species. This was facilitated by introducing the $Nb(OEt)_5$ to a prehydrolyzed, loosely-bonded silica gel, and then further stirring and aging the mixture at room temperature to maximize the homogeneity of the mixture. We further note that the specific surface area decreased with increased Nb concentration, which could be attributed to the larger Nb atomic weight and the reduced regularity of the pore packing.

Effects of Sol pH and Surfactant Concentration. Self-assembly of the inorganic and organic species in the gel solution into a well-ordered mesostructure only occurs by proper charge matching, which can be tuned by the pH of the reaction medium. Using TMAS as a siliceous source, the mesostructure can be obtained at a pH range of 7-12 (Figure 6); however, the intensity of XRD pattern decreased with pH decrease. At around neutral pH, the charges on the oligomeric silica species were substantially lowered, weakening the driving force for self-assembly: $pH \leq 5$ led to amorphous oxide gels due to rapid reaction of $Nb(OEt)_5$ and silicate precursors.

The surfactant chemistry is critical to the formation of mesostructure. Previous work in silica-based M41S materials showed that hexagonal, cubic and lamellar structures could be formed by increasing the surfactant-to-Si ratio in the precursor sol of pH = 10 at 150°C (Beck et al., 1992, 1994; Vartuli et al., 1994). In this study, the surfactant/Si ratio was

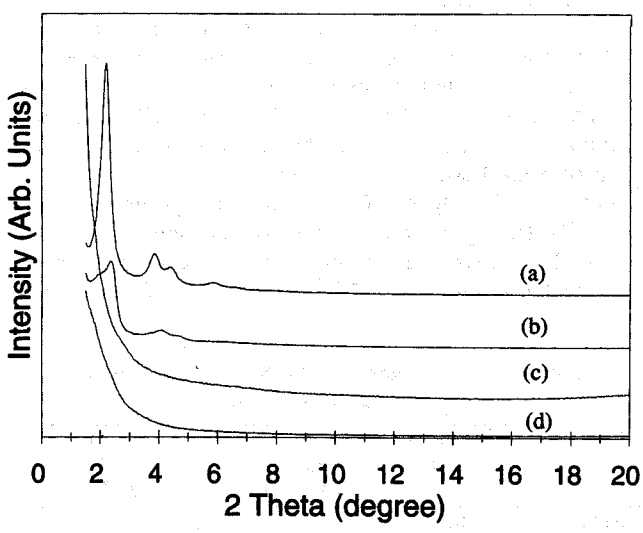

Figure 6. XRD patterns of NbSi1-20 samples obtained at a pH of (a) 11.5, (b) 7, (c) 5, and (d) 1.

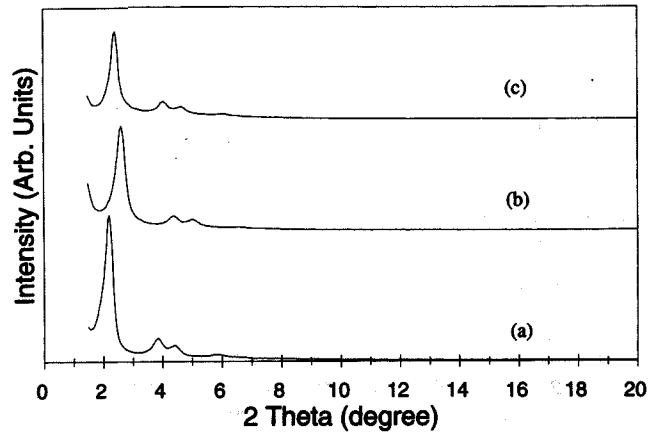

Figure 7. XRD patterns of NbSi1-20 samples synthesized with a surfactant-to-Si ratio of (a) 0.5, (b) 1, and (c) 2.

varied between 0.5 and 2 in the synthesis of NbSi1-20, and the resulting XRD patterns of all calcined samples exhibited a hexagonal structure (Figure 7). The presence of the Nb precursors in the reaction medium under these conditions appears to favor the hexagonal phase despite the significant variation in the surfactant/Si ratio. The incorporation of Nb dopants might have interfered with the interaction between inorganic and organic species. We noted a decrease of the d-spacing at a surfactant-to-Si ratio of 1, which may imply that the structural rearrangement occurs at different surfactant concentrations. The detail mechanism is unclear at this stage.

The TGA analysis of the Nb-doped samples showed two stages of weight loss in air, resulting from the removal of water at lower temperatures ($T < 150$°C) and the decomposition of the surfactants at 250–300°C. A greater weight loss was found in the samples prepared with higher surfactant-to-Si ratios.

Effects of Aging Temperature and Addition of a Swelling Agent. Analysis of the thermal evolution of the mesoporous structure indicated that the mesophases could undergo a restructuring process, with stability and pore characteristic being controlled by kinetic parameters such as aging temperature. The structural transformation was affected by entropic changes in the organic array and also the rearrangement of the inorganic species (Stucky et al., 1996). Under basic conditions, dissolution and reprecipitation of the partial silica framework can occur at high temperatures over an extended reaction period. The soluble silica species are transported to and redeposited at regions of high curvature, further expanding the pore size (Khushalani et al., 1995). Increasing the temperature during synthesis can accelerate the condensation of the inorganic precursor and rearrange the mesostructure. This study found that the pore packing and structure of the Nb-doped mesoporous silicas could be controlled by varying the aging temperature (see Figure 8). The $d(100)$ spacing increased with an increase in the aging temperature. The higher order peaks became better resolved and increased in intensity with increasing aging temperature, showing an improvement in the long-range pore packing of the materials. The average BJH pore sizes of the resulting materials were

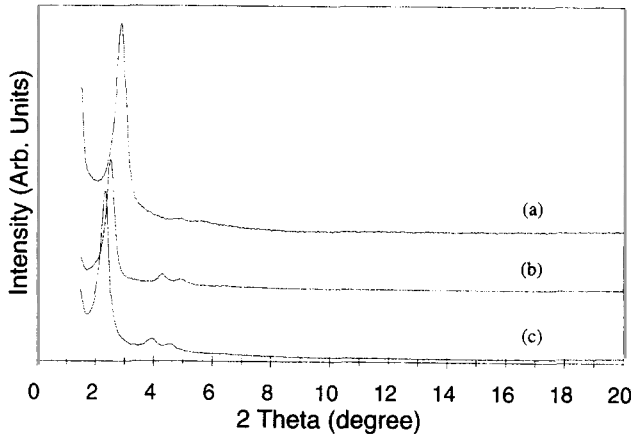

Figure 8. XRD patterns of the NbSi2-20 samples aged for 36 hours at (a) 25°C, (b) 100°C, and (c) 150°C.

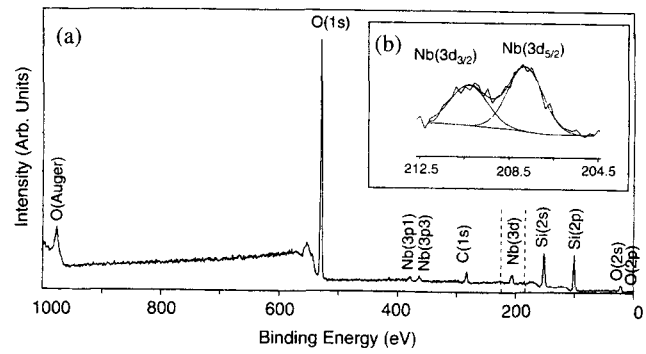

Figure 9. XPS spectrum of NbSi1-10: (a) the full spectrum and (b) the section of the spectrum showing the Nb(3d) peaks which are fitted with a Gaussian distribution.

observed to increase from 17Å to 23Å as the reaction temperature was elevated from 25°C to 150°C.

To obtain even larger pore diameters, organic swelling agents can be introduced during synthesis. When the hydrophobic molecules such as mesitylene are added, they are incorporated in the hydrophobic micellar cores to produce MCM-41 with pores > 40 Å (Beck et al., 1992). In this study, an as-prepared sample made with two equivalents of mesitylene gave a large $d(100)$ spacing of 52.5 Å, but the pore packing in the mesostructure was less defined and the pore size distribution was broadened. It was found that the pore size could not be increased beyond 50Å with mesitylene addition for the Nb-doped silicates.

In general, the microstructure of mesoporous Nb-doped silicas depends strongly on the siliceous source, Nb dopant concentration, pH of the medium, and aging temperature. The synthesis conditions can be controlled to tailor the microstructure of the materials toward the desired application.

Nature of the Nb-dopants in the mesoporous silica

Knowledge of the location and coordination of the transition metal cations in the framework of the mesostructure is of practical importance and could lead to a better understanding of the synthesis process and the mechanism of catalytic reactions.

XPS and EPR Studies. XPS provides a compositional analysis of the surface of materials. The XPS spectra of the calcined Nb-doped mesoporous silica primarily showed the energy absorption from Si, Nb and O elements (Figure 9a). Some O Auger electrons were noted at higher binding energy. The binding energy of Nb(3d) was obtained from the deconvolution of the Nb($3d_{3/2}$) and Nb($3d_{5/2}$) photoelectron peaks (Figure 9b). The results (Table 3) agreed with previously reported binding energy data for Nb_2O_5 (McGuire et al., 1973; Simon et al., 1976; Fontaine et al., 1977) and SiO_2-supported Nb_2O_5 catalyst (Weissman et al., 1987). The difference between the binding energy of Nb($3d_{3/2}$) and Nb($3d_{5/2}$) was about 2.6 eV, comparable with that of Nb_2O_5 (Wagner et al., 1992). These results indicated the presence of Nb^{5+} sites in the mesoporous Nb-doped silica materials. The asymmetry of the O(1s) photoelectron peak suggested the presence of Nb-O-Si linkage. The Nb oxidation state was also confirmed by the EPR study. The absence of an EPR signal related to Nb^{5+} species could be explained by the diamagnetic property of Nb^{5+} sites (Mabbs et al., 1992).

FTIR and UV-Vis Studies. PA-FTIR spectroscopy provides information on molecular bonding of the material. The spectra of the mesoporous materials (Figure 10) illustrate the characteristic asymmetric Si-O-Si backbone phonon vibration bands at 960 – 1,280 cm^{-1} and symmetric stretchings at 760 – 880 cm^{-1} of the SiO_2 matrix (Ying et al., 1993). Compared to a pure mesoporous silica, the slight shift of both the symmetric and asymmetric bands might be an indication of Nb incorporation into the silica framework. The Si-OH feature at 978 cm^{-1} was broadened and increased in intensity with increasing Nb dopant concentration. This may be related to the vibrational bands of the dopant component, since the PA-FTIR spectrum of pure Nb_2O_5 shows a broad absorption band starting at 960 cm^{-1}. Similar results were also reported for the Ti-MCM-41 and V-MCM-41 systems (Bellussi et al., 1994; Hari Prasad Rao et al., 1993). Although the origin and assignment of the band are still in debate, the peak broadening can be attributed to the distorted local Nb characteristics in the Si-O-Nb bond.

Pyridine bonds with Lewis acid sites, giving IR characteristic bands at ~1,610 cm^{-1} and 1,450 cm^{-1}. Brønsted acid sites are represented by the band near 1,550 cm^{-1} and two weak bands at 1,620 – 1,640 cm^{-1}. *In-situ* DRIFT studies with pyridine adsorption on NbSi1-20 sample indicated the presence of weak Lewis acid sites and negligible Brønsted acid sites (Figure 11). By 300 °C, desorption of pyridine was complete, illustrating the weakness of the acid sites in these materials. The Lewis acidity is attributed to the surface-exposed coordinatively-unsaturated Nb^{5+} sites or extra framework Nb

Table 3. Binding Energy of the Nb Atom in Nb-Doped Mesoporous Silicate

	Nb($3d_{5/2}$) Binding Energy (eV)	Nb($3d_{3/2}$) Binding Energy (eV)	Energy Diff. (eV) Nb($3d_{3/2}$) – Nb($3d_{5/2}$)
NbSi1-10	207.8	210.4	2.6
NbSi2-10	207.9	210.6	2.7
NbSi3-10	207.5	210.1	2.6

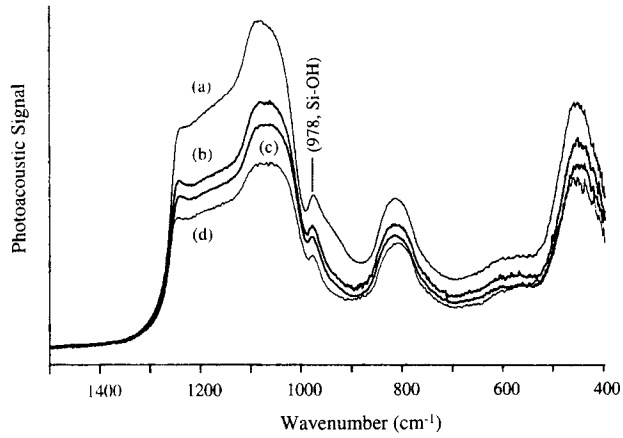

Figure 10. PA-FTIR spectra of (a) NbSi1-10, (b) NbSi1-20 and (c) NbSi1-100, and (d) pure mesoporous silica.

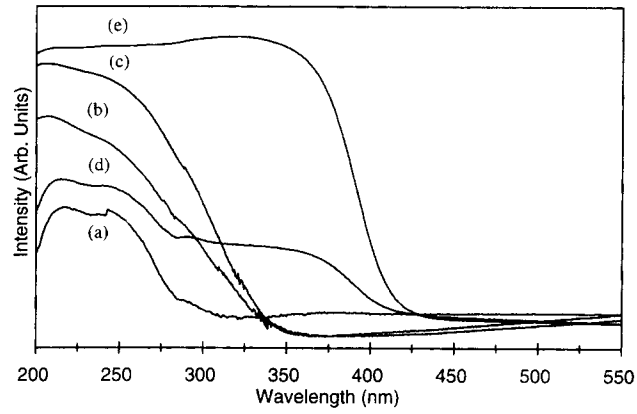

Figure 12. Diffuse-reflectance UV-Vis spectra of (a) pure mesoporous silica, (b) NbSi1-100, (c) NbSi1-10, (d) physical mixture of mesoporous silica and Nb_2O_5, and (e) Nb_2O_5.

species. It was reported that the introduction of a high Nb dopant concentration improved the Brønsted acidity of the H^+-form of Nb-MCM-41 materials (Ziolek et al., 1997). Such weak acidity may be useful in catalytic applications, such as synthesis of methanethiol from CH_3OH and H_2S (Ziolek et al., 1997).

Compared to the UV-Vis spectrum of mesoporous pure silica with an absorption edge at 270 nm (Figure 12a), the significant red shift noted with the introduction of Nb dopants could be related to the mixed valence states of the Nb and Si affecting the band energy of the mesoporous materials. This shift to higher wavelength increased with increasing Nb dopant concentration. The absorption edge of pure Nb_2O_5 is near 410 nm (Figure 12e). The UV-Vis spectra have two small absorption peaks at 210 nm and 245 nm for materials with low Nb-dopant concentrations (Figure 12b). These peaks were greatly broadened at higher dopant levels presumably due to a ligand-to-metal charge transfer. In these materials, the Nb cations are coordinated to four oxygen atoms, but because of their large covalent radius, they can interact with one or two H_2O molecules, thereby creating a distorted tetrahedral environment. In a SiO_2-supported Nb_2O_5 catalyst, the charge transfer band of tetrahedral Nb(V) = 0 was observed at 235 nm (Nishimura et al., 1986). The spectra of V-MCM-41 exhibited similar bands near this wavelength, which are attributed to the charge transfer bands of V(V) in the tetrahedral coordination (Morey et al., 1996; Carvalho et al., 1997). The spectrum of a physical mixture of mesoporous pure silica and pure Nb_2O_5 (50:50 wt. ratio) showed two distinct absorption edges corresponding to silica (270 nm) and niobium oxide (410 nm), respectively. In contrast, the UV-Vis spectra of the Nb-doped mesoporous silica showed a single, smooth absorption edge, suggesting a homogeneous dispersion of Nb dopants throughout the silica framework.

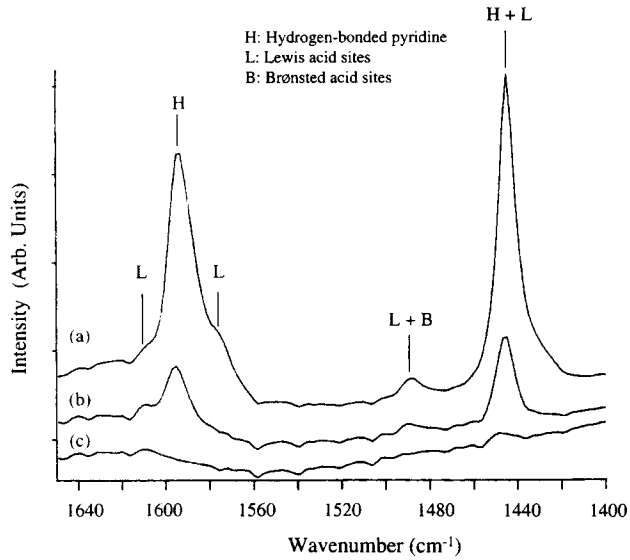

Figure 11. *In-situ* DRIFT spectra of NbSi1-20 sample at (a) 150°C saturated with pyridine, (b) 150°C after 30 min of purging with He, and (c) 300°C after 30 min of purging with He.

^{29}Si MAS NMR Studies. The NMR technique is highly sensitive to the local coordination of detectable species. There is great difficulty in studying our materials with ^{93}Nb NMR, however, due to the large chemical shift and quadrupole interaction of the Nb nuclei (Redder et al., 1991). We have consequently utilized ^{29}Si MAS NMR since the possible coupling of Nb to Si can be detected in the molecular structure of silica. The spectrum of a NbSi1-1.33 sample (Figure 13b) closely resembles that of the mesoporous pure silica sample (Figure 13a). In addition to the Q^4 peak (SiO_4 unit) at approximately -108 ppm and a minor Q^3 peak [SiO_3(OH) unit] at about -98 ppm, the spectrum of NbSi-1.33 sample also showed a very broad component at about -105 ppm. This may be attributed to the effect of Si bonding with Nb and therefore can be the evidence for Si-O-Nb bonding in the structure. This component can be seen more clearly as the negative peak in the difference spectrum (Figure 13c). The spectra of NbSi1-10 and NbSi1-20 both presented a weak broad peak in the range of -103 to -105 ppm. A similar broad peak at -106 ppm was observed in previous studies of mesoporous metal-doped silicate materials and was attributed to framework M-O-Si bondings (Cheng et al., 1996; Carvalho et al., 1997).

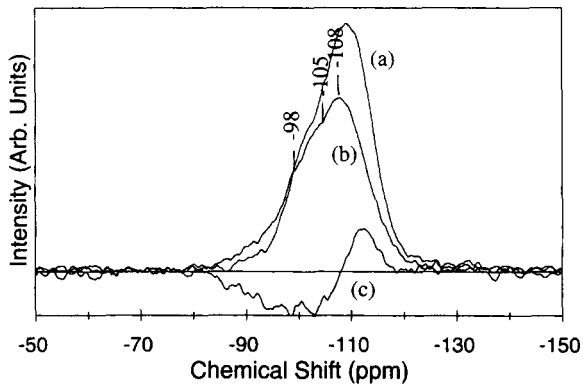

Figure 13. ^{29}Si MAS NMR spectra of (a) pure mesoporous silica, (b) NbSi1-1.33, and (c) difference spectrum of (a) and (b).

Conclusions

Mesoporous Nb-doped silica materials have been successfully synthesized through a micellar templating route. The microstructure of this system can be tailored by controlling various synthesis parameters. The quality and characteristics of the materials depend on the siliceous precursor, dopant concentration, sol pH, and aging temperature. It was shown that Nb species were incorporated into the framework of hexagonally-packed mesoporous silica at concentration as high as ~ 10 wt. %. The XPS studies indicated the presence of Nb^{5+} sites in the mesoporous doped silica. The ^{29}Si MAS NMR spectrum of the material showed a new broad peak at −105 ppm, suggesting the formation of Nb-O-Si bonding in the mesostructure.

Acknowledgments

This work is supported by the David and Lucile Packard Foundation and the National Science Foundation (CTS-9257223). Z. Zhang and M. S. Wong (M.I.T.) are acknowledged for their assistance in the TEM studies. The authors would like to thank M. S. Wong for helpful discussions.

Literature Cited

Alquier, C., M. T. Vandenborre, and M. Henry, "Synthesis of Niobium Pentoxides Gels," *J. Non-Cryst. Solids*, **79**, 383 (1986).

Antonelli, D. M., A. Nakahira, and J. Y. Ying, "Ligand-Assisted Liquid Crystal Templating in Mesoporous Niobium Oxide Molecular Sieves," *Inorg. Chem.*, **35**, 3126 (1996).

Antonelli, D. M., and J. Y. Ying, "Mesoporous Materials," *Curr. Op. Coll. Interf. Sci.*, **1**, 523 (1996a).

Antonelli, D. M., and J. Y. Ying, "Synthesis of Stable Hexagonally-Packed Mesoporous Niobium Oxide Molecular Sieves Through a Novel Ligand-Assisted Templating Mechanism," *Angew. Chem. Int. Ed. Engl.*, **35**, 426 (1996b).

Barrett, E. P., L. G. Joyner, and P. P. Halenda, "The Determination of Pore Volume and Area Distribution in Porous Substances. I. Computations from Nitrogen Isotherms," *J. Amer. Chem. Soc.*, **73**, 373 (1951).

Beard, W. C., "Infrared Studies of Aqueous Silicate Solutions," *Molecular Sieves*, R. F. Gould, ed., Amer. Chem. Soc., p. 162 (1973).

Beck, J. S., J. C. Vartuli, W. J. Roth, M. E. Leonowicz, C. T. Kresge, K. D. Schmitt, C. T.-W. Chu, D. H. Olsen, E. W. Sheppard, S. B. McCullen, J. B. Higgins, and J. L. Schlenker, "A New Family of Mesoporous Molecular Sieves Prepared with Liquid Crystal Templates," *J. Amer. Chem. Soc.*, **114**, 10,834 (1992).

Beck, J. S., J. C. Vartuli, G. J. Kennedy, C. T. Kresge, W. J. Roth, and S. E. Schramm, "Molecular or Supramolecular Templating: Defining the Role of Surfactant Chemistry in the Formation of Microporous and Mesoporous Molecular Sieves," *Chem. Mater.*, **6**, 1816 (1994).

Bellussi, G., and M. S. Rigutto, "Advanced Zeolite Science and Applications," *Stud. Surf. Sci. Catal.*, **85**, 177 (1994).

Brack, D. W., and E. M. Flanigan, *Molecular Sieves*, Soc. of Chem. Ind., p. 47 (1968).

Brinker, C. J., "Porous Inorganic Materials," *Curr. Op. Solid State Mater. Sci.*, **1**, 798 (1996).

Brinker, C. J., and G. W. Scherer, *Sol-Gel Science: The Physics and Chemistry of Sol-Gel Processing*, Academic Press, Boston (1990).

Carvalho, W. A., P. B. Varaldo, M. Wallu, and U. Schuchardt, "Mesoporous Redox Molecular Sieves Analogous to MCM-41," *Zeolites*, **18**, 408 (1997).

Chen, C.-Y., S. L. Burkett, H.-X. Li, and M. E. Davis, "Studies on Mesoporous Materials: II. Synthesis Mechanism of MCM-41," *Microporous Mater.*, **2**, 27 (1993).

Cheng, C. F., H. He, W. Zhou, J. Klinowski, J. A. Sousa Gonçalves, and L. F. Gladden, "Synthesis and Characterization of the Gallosilicate Mesoporous Molecular Sieve MCM-41," *J. Phys. Chem.*, **100**, 390 (1996).

Corma, A., M. T. Navarro, and J. Pérez Pariente, "Synthesis of an Ultralarge Pore Titanium Silicate Isomorphous to MCM-41 and its Application as a Catalyst for Selective Oxidation of Hydrocarbons," *J. Chem. Soc., Chem. Commun.*, 147 (1994).

Faiberother, F., *The Chemistry of Niobium and Tantalum*, Elsevier, Amsterdam (1967).

Firouzi, A., D. Kumar, L. M. Bull, T. Besier, P. Sieger, Q. Huo, S. A. Walker, J. A. Zasadzinski, C. Glinka, J. Nicol, D. Margolese, G. D. Stucky, and B. F. Chmelka, "Cooperative Organization of Inorganic-Surfactant and Biomimetic Assemblies," *Science*, **267**, 1138 (1995).

Fontaine, R., R. Callat, L. Feve, and M. J. Guittet, "Déplacement Chimique ESA Dans la Série Des Oxydes Du Niobium," *J. Elect. Spectros.*, **10**, 349 (1977).

Gregg, S. K., and K. S. W. Sing, *Adsorption, Surface Area and Porosity*, Academic Press, London (1982).

Hari Prasad Rao, P. R., R. Kumar, A. V. Ramaswamy, and P. Ratnasamy, "Synthesis and Characterization of a Crystalline Vanadium Silicate with MEL Structure," *Zeolites*, **13**, 663 (1993).

Huo, Q., D. I. Margolese, U. Ciesla, D. G. Demuth, P. Feng, T. E. Gier, P. Sieger, A. Firouzi, B. F. Chmelka, F. Schüth, and G. D. Stucky, "Organization of Organic Molecules with Inorganic Molecular Species into Nanocomposite Biphase Arrays," *Chem. Mater.*, **6**, 1176 (1994a).

Huo, Q., D. I. Margolese, U. Ciesla, P. Feng, T. E. Gier, P. Sieger, R. Leon, P. M. Petroff, F. Schüth, and G. D. Stucky, "Generalized Synthesis of Periodic Surfactant/Inorganic Composite Materials," *Nature*, **368**, 317 (1994b).

Huo, Q., R. Leon, P. M. Petroff, and G. D. Stucky, "Mesostructure Design with Gemini Surfactants: Supercage Formation in a Three-Dimensional Hexagonal Array," *Science*, **268**, 1324 (1995).

Huo, Q., D. I. Margolese, and G. D. Stucky, "Surfactant Control of Phases in the Synthesis of Mesoporous Silica-Based Materials," *Chem. Mater.*, **8**, 1147 (1996).

Iler, R. K., *The Chemistry of Silica*, Wiley, New York, p. 150 (1979).

Khushalani, D., A. Kuperman, G. A. Ozin, K. Tanaka, J. Garces, M. M. Olken, and N. Coombs, "Metamorphic Materials: Restructuring Siliceous Mesoporous Materials," *Adv. Mater.*, **7**, 842 (1995).

Kresge, C. T., M. E. Leonowicz, W. J. Roth, J. C. Vartuli, and J. S. Beck, "Ordered Mesoporous Molecular Sieves Synthesized by a Liquid-Crystal Template Mechanism," *Nature*, **359**, 710 (1992).

Liu, C.-C., X.-K. Ye, and Y. Wu, "Hydroxylation of Phenol by Iron(II)-Phenanthroline/MCM-41 Zeolite," *Catal. Lett.*, **36**, 263 (1996).

Luan, Z. H., C. F. Cheng, W. Z. Zhou, and J. Klinowski, "Mesoporous Molecular Sieve MCM-41 Containing Framework Aluminum," *J. Phys. Chem.*, **99**, 1018 (1995).

Mabbs, F. E., and D. Collison, "Electron Paramagnetic Resonance of d Transition Metal Compounds," *Stud. Inorg. Chem.*, **16** (1992).

McGuire, G. E., G. K. Schweitzer, and T. A. Carlson, "Study of Core Electron Binding Energies in Some Group IIIa, Vb, and VIb Compounds," *Inorg. Chem.*, **12**, 2451 (1973).

Morey, M., A. Davidson, H. Eckert, and G. D. Stucky, "Pseudotetrahedral $O_{3/2}V=0$ Centers Immobilized on the Walls of a Mesoporous Cubic MCM-48 Support: Preparation, Characterization and Reactivity toward Water as Investigated by ^{51}V NMR and UV-Vis Spectroscopies," *Chem. Mater.*, **8**, 486 (1996).

Nishimura, M., K. Asakura, and P. Iwasawa, "New SiO_2-Supported Niobium Monomer Catalysts for Dehydrogenation of Ethanol," *J. Chem. Soc., Chem. Commun.*, 1660 (1986).

Oster, G., and D. P. Riley, "Scattering from Cylindrically Symmetric Systems," *Acta Cryst.*, **5**, 272 (1952).

Redder, D., "Transition Metal Nuclear Magnetic Resonance," *Stud. Inorg. Chem.*, **13**, 45 (1991).

Reddy, K. M., I. L. Moudrakouski, and A. Sayari, "Synthesis of Mesoporous Vanadium Silicate Molecular Sieves," *J. Chem. Soc., Chem. Commun.*, 1059 (1994).

Sayari, A., "Catalysis by Crystalline Mesoporous Molecular Sieves," *Chem. Mater.*, **8**, 1840 (1996).

Sayari, A., C. Danumah, I. L. Moudrakouski, A. I. Ratcliffe, J. A. Ripmeester, and K. F. Preston, "Synthesis and Nuclear Magnetic Resonance Study of Boron-Modified MCM-41 Mesoporous Materials," *J. Phys. Chem.*, **99**, 16,373 (1995).

Schacht, S., Q. Huo, I. G. Voigt-Martin, G. D. Stucky, and F. Schüth, "Oil-Water Interface Templating of Mesoporous Macroscale Structures," *Science*, **273**, 768 (1996).

Schwarz, S., D. R. Corbin, and A. J. Vega, "The Band at 960," *Mater. Res. Soc. Sym. Proc.*, **431**, 137 (1996).

Simon, D., C. Perrin, and P. Baillif, "Electron Spectrometric Study (ESCA) of Niobium and Its Oxides. Application to Its Oxidation at High Temperature and Low Oxygen Pressure," *C. R. Acad. Sci. Paris*, **283C**, 241 (1976).

Stucky, G. D., Q. Huo, A. Firouzi, B. F. Chmelka, S. Schacht, I. G. Voigt-Martin, and F. Schüth, "Directed Synthesis of Organic/Inorganic Composite Structures," *Stud. Surf. Sci. Catal.*, **105**, 3 (1996).

Tanev, P. T., M. Chibwe, and T. J. Pinnavaia, "Titanium-Containing Mesoporous Molecular Sieves for Catalytic Oxidation of Aromatic Compounds," *Nature*, **368**, 321 (1994).

Tanev, P. T., and T. J. Pinnavaia, "A Neutral Templating Route to Mesoporous Molecular Sieves," *Science*, **267**, 865 (1995).

Tanev, P. T., and T. J. Pinnavaia, "Mesoporous Silica Molecular Sieves Prepared by Ionic and Neutral Surfactant Templating: A Comparison of Physical Properties," *Chem. Mater.*, **8**, 2068 (1996).

Vartuli, J. C., K. D. Schmitt, C. T. Kresge, W. J. Roth, M. E. Leonowicz, S. B. McCullen, S. D. Hellring, J. S. Beck, J. L. Schlenker, D. H. Olsen, and E. W. Sheppard, "Effect of Surfactant/Silica Molar Ratios on the Formation of Mesoporous Molecular Sieves: Inorganic Mimicry of Surfactant Liquid-Crystal Phases and Mechanistic Implications," *Chem. Mater.*, **6**, 2317 (1994).

Wagner, C. D., W. M. Riggs, L. E. Davis, J. F. Moulder, and G. E. Muilenberg, "Handbook of X-Ray Photoelectron Spectroscopy," Physical Electronics Div., Perkin-Elmer Corp., Eden Prairie, MN (1992).

Weissman, J. G., E. I. Ko, and P. Wynblatt, "Study of the Morphology and Structure of Niobium-Silica Surface Oxide Using Model Thin Films," *J. Catal.*, **108**, 383 (1987).

Wu, C.-G., and T. Bein, "Polyaniline Wires in Oxidant-Containing Mesoporous Channel Hosts," *Chem. Mater.*, **6**, 1109 (1994).

Yang, H., A. Kuperman, N. Coombs, S. Mamiche-Afara, and G. A. Ozin, "Synthesis of Oriented Films of Mesoporous Silica on Mica," *Science*, **379**, 703 (1996).

Ying, J. Y., J. B. Benziger, and A. Navrotsky, "Structural Evolution of Alkoxide Silica Gels to Glass: Effect of Catalyst pH," *J. Amer. Ceram. Soc.*, **76**, 2571 (1993).

Yuan, Z. Y., S. Q. Liu, T. H. Chen, Z. J. Wang, and H. X. Li, "Synthesis of Iron-Containing MCM-41," *J. Chem. Soc., Chem. Commun.*, 973 (1995).

Zhang, L., T. Sun, and J. Y. Ying, "A Rationally-Designed Oxidation Catalyst: Functionalized Metalloporphyrin Encapsulated in a Transition Metal-Doped Mesoporous Silica," *Catal. Lett.*, submitted (1997).

Zhang, W., J. Wang, P. T. Tanev, and T. J. Pinnavaia, "Catalytic Hydroxylation of Benzene over Transition-Metal Substituted Hexagonal Mesoporous Silicas," *Chem. Commun.*, 979 (1996).

Zhao, D., and D. Goldfarb, "Synthesis of Manganosilicates: Mn-MCM-41, Mn-MCM-48 and Mn-MCM-L," *J. Chem. Soc., Chem. Commun.*, 875 (1995).

Zhao, X. S., G. Q. Lu, and J. M. Graeme, "Advances in Mesoporous Molecular Sieve MCM-41," *Ind. Eng. Chem. Res.*, **35**, 2075 (1996).

Ziolek, M., I. Nowak, and J. C. Lavalley, "Acidity Study of Nb-Containing MCM-41 Mesoporous Materials: Comparison with that of Al-MCM-41," *Catal. Lett.*, **45**, 259 (1997).

Manuscript received May 16, 1997, and revision received Sept. 16, 1997.